Interaction of oscillatory and excitable localized states in a nonlinear optical cavity

Damià Gomila, Adrián Jacobo, Manuel A. Matías, and Pere Colet

Abstract The interaction between stationary localized states have long been studied, but localized states may undergo a number of instabilities that lead to more complicated dynamical regimes. In this case, the effects of the interaction are much less known. This chapter addresses the problem of the interaction between oscillatory and excitable localized states in a Kerr cavity. These oscillatory structures can be considered as non punctual oscillators with a highly non-trivial spatial coupling, which leads to rather complicated dynamics beyond what can be explained in terms of simple coupled oscillators. We also explore the possibility of using coupled excitable localized structures to build all-optical logical gates.

1 Introduction

Localized states (LS) are commonplace in extended system exhibiting bistability between two different solutions [1]. Physically they imply an equilibrium in a finite region in space between dissipation and driving, and nonlinearity and diffusion. In the nonlinear optics context the spatial coupling is mainly given by diffraction, although diffusion can be also present in some cases.

All these ingredients are present in optical cavities filled with a nonlinear medium [2, 3]. The driving is given by a broad homogeneous holding beam which is shined on a semi-reflecting mirror of the cavity. Part of the light will be reflected, but the rest enters the cavity. If the holding beam is switched off all the energy leave the cavity through the same semi-reflecting mirror, which makes the system dissipative. The spatial coupling is provided by the diffraction of the propagating light, which smoothes out any spatial inhomogeneity. Finally, a nonlinear medium provides the necessary photon-photon interactions to observe a complex behavior such as the formation of localized states.

IFISC, Instituto de Física Interdisciplinar y Sistemas Complejos (CSIC-UIB), Campus Universitat Illes Balears, 07122 Palma de Mallorca, Spain, e-mail: damia@ifisc.uib-csic.es

Nonlinear optical cavities have long been shown to support localized states, and stationary LS have been advocated for their use as bits in optical memories [4, 5]. An important feature of these LS is that they interact through their oscillatory tails in such a way that they anchor at a discrete set of distances [6, 7, 8]. But LS can also undergo a number of instabilities leading to more complicated dynamical regimes [9, 10]. In this case the role of the interaction is much less known. In particular, we will focus here on the study of the interaction of oscillatory and excitable LS in a Kerr cavity. In this system the dynamics of LS is an intrinsic property of the coherent structures that emerges from the spatially extended nature of the system. Thus, for instance, oscillatory LS are non-punctual oscillators, i.e. oscillators with internal structure or degrees of freedom. As a result, their interaction can not necessarily be reduced to a simple coupling term between punctual oscillators. The interplay between the oscillatory dynamics, the interaction, and the internal structure can affect the dynamics in a nontrivial way. This chapter is an attempt to address this general problem by studying a prototypical case.

2 Model

We study the dynamics and interaction of localized states in a prototypical model, namely the Lugiato-Lefever equation, describing the dynamics of the slowly varying envelope $E(\mathbf{x},t)$ of the electric field in a ring cavity filled with a self-focusing Kerr medium (see Figure 1). In the mean field approximation, where the dependence of the field on the longitudinal direction has been averaged, and in the paraxial limit, the dynamics of E in two transverse spatial dimensions is described by the following equation [11]:

$$\frac{\partial E}{\partial t} = -(1+i\theta)E + i\nabla^2 E + E_{in} + i|E^2|E, \tag{1}$$

where $\mathbf{x} = (x,y)$ is the transverse plane and $\nabla^2 = \partial^2/\partial x^2 + \partial^2/\partial y^2$. The first term on the right-hand side describes the cavity losses, rescaled to 1, E_{in} is the input field, and θ the cavity detuning with respect to input field. Space, time, and the field have been suitable rescaled so that Eq. (1) is dimensionless. This model was one of the first proposed to study pattern formation in nonlinear optics [11], and it was shown later that LS are also observed in some parameter regions [12, 13].

It is important to note that in the absence of losses and input, the intra-cavity field can be rescaled ($E \to Ee^{i\theta t}$) to remove the detuning term and (1) becomes the nonlinear Schrödinger equation (NLSE). As it will be explained later in more detail, the dynamics of LS in this system is connected with the collapse of the 2D solitons in the NLSE.

Equation (1) has a homogeneous steady-state solution which is implicitly given by $E_s = E_{in}/[1+(i(\theta - I_s)]$, where $I_s = |E_s|^2$. For convenience, we will use in the following the intra-cavity background intensity I_s, together with θ, as our control parameters. It is well known that the homogeneous solution shows bistability for $\theta > \sqrt{3}$. Here we will restrict ourselves to $\theta < \sqrt{3}$ so that I_s is unique once E_{in} is

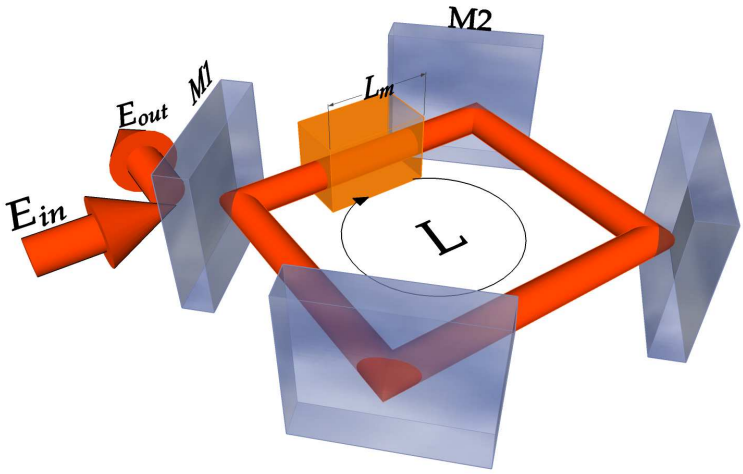

Fig. 1 Ring cavity of length L filled with a nonlinear medium of length L_m. Mirror M1 is only partially reflecting, so that the cavity can be driven by E_{in} and read out with E_{out}.

determined. For $I_s > 1$ the homogeneous solution is modulationally unstable and dynamical hexagonal patterns are formed. The bifurcation is subcritical and stationary hexagonal patterns are stable below threshold [14, 15]. In this situation, LS typically exist and their dynamics and interactions are the subject of study in the rest of this chapter.

3 Overview of the behavior of localized states

The bistability of the pattern and homogeneous solutions is at the origin of the existence of stable LS that appear when suitable (localized) transient perturbations are applied. The LS can be seen as a solution which connects a cell of the pattern with the homogeneous solution. While the existence of LS in this bistable regime is quite generic in extended systems [16, 17], their stability strongly depends on the particularities of the system. Using a Newton method it is possible to find the stationary LS solutions with arbitrary precision and determine their stability by diagonalizing the Jacobian. Complemented with numerical simulations, this method allows to gain insight into the structure of the phase space of the system [18, 19, 1].

3.1 Hopf bifurcation

Early studies already identified that LS may undergo a Hopf bifurcation leading to a oscillatory behavior [12]. The oscillatory instabilities [20], as well as azimuthal

instabilities, were fully characterized later [10]. Interestingly, the oscillations of the LS show the connection of Eq. (1) with the NLSE. The growth of an LS during the oscillations resembles the collapse regime observed for solitons in the $2D$ (or $2+1$) NLSE. In this case, however, after some value is attained for the electric field, E, dissipation arrests this growth. This also explains why, despite LS are also observed in 1D [21], oscillations are not present in that case, since collapse does not occur in the 1D NLSE.

As one moves in parameter space away from the Hopf bifurcation, the LS oscillation amplitude grows and its frequency decreases. Eventually, the limit cycle touches the middle-branch LS in a saddle-loop bifurcation which leads to a regime of excitable dissipative structures [22, 19]. In the next two subsections we briefly explain the saddle-loop bifurcation and the excitable regime. For an extensive analysis of this scenario see, for instance, Ref. [1].

3.2 Saddle-loop bifurcation

A saddle-loop or homoclinic bifurcation is a global bifurcation in which a limit cycle becomes biasymptotic to a saddle point, or, in other terms, becomes the homoclinic orbit of the saddle, i.e., at criticality a trajectory leaving the saddle point through the unstable manifold returns to it through the stable manifold. Thus, at one side of this bifurcation one finds a detached limit cycle (stable or unstable), while at the other side the cycle does not exist any more, only its *ghost*, as the bifurcation creates an exit slit that makes the system dynamics to leave the region in phase space previously occupied by the cycle. Therefore, after the bifurcation the system dynamics jumps to another available attractor. In the present case this alternative attractor is the homogeneous solution.

The fact that the bifurcation is global, implies that it cannot be detected locally (a local eigenvalue passing through zero), but one can still resort to the Poincaré map technique to analyze it, and, interestingly, the main features of the bifurcation can be understood from the knowledge of the linear eigenvalues of the saddle [23]. The case studied here is the simplest: a saddle point with real eigenvalues, in a 2-dimensional phase space. Strictly speaking, in our case the saddle has an infinite number of eigenvalues, but only two eigenmodes take part in the dynamics close to the saddle [19].

To identify such a transition one can study the period of the cycle close to this bifurcation, and to leading order it must be given by [24],

$$T \propto -\frac{1}{\lambda_u} \ln|\theta - \theta_c| \,, \tag{2}$$

where λ_u is the unstable eigenvalue of the saddle and θ_c the critical value of the detuning. Numerically the bifurcation point is characterized by the fact that approaching from the oscillatory side the period diverges to infinity, and also because past

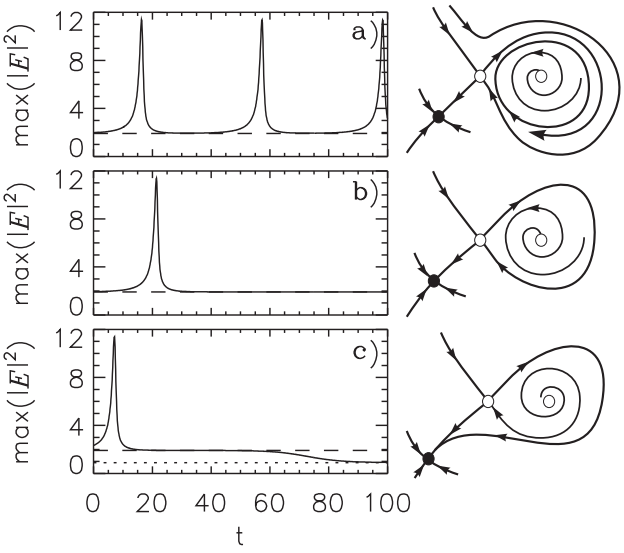

Fig. 2 Left: time evolution of the maximum of the LS plotted for three different values of the detuning: a) just below, b) at the saddle-loop bifurcation, and c) just above. Right: sketch of the phase space for each situation.

this bifurcation point the LS disappears and the system relaxes to the homogeneous solution as shown in Fig. 2.

A logarithmic-linear plot of the period versus the control parameter exhibits a linear slope according to the theoretical prediction (2), whit λ_u obtained from the linear stability analysis of the saddle [19].

3.3 Excitability

As in our case the saddle-loop bifurcation involves a fixed point (the homogeneous solution), on one side of the bifurcation, and an oscillation, on the other, the system is a candidate to exhibit excitability [25]. It must be stressed that excitable behavior is not guaranteed *per se* after a saddle-loop bifurcation, and, in particular one needs a fixed point attractor that is close enough to the saddle point that destroys the oscillation. The excitability threshold in this type of systems is the stable manifold of the saddle point, what implies that the observed behavior is formally Class I Excitability [25].

This excitability scenario was first shown in Ref. [22]. Fig. 3 shows the resulting trajectories after applying a localized perturbation in the direction of the unstable LS with three different amplitudes: one below the excitability threshold, and two above, one very close to threshold and another well above. For the one below threshold

the perturbations decays exponentially to the homogeneous solution, while for the two above threshold a long excursion in phase space is performed before returning to the stable fixed point. The refractory period for the perturbation just above the excitability threshold is appreciably longer due to the effect of the saddle. After an initial localized excitation is applied, the peak grows to a large value until the losses stop it. Then it decays exponentially until it disappears. A remnant wave is emitted out of the center dissipating the remaining energy.

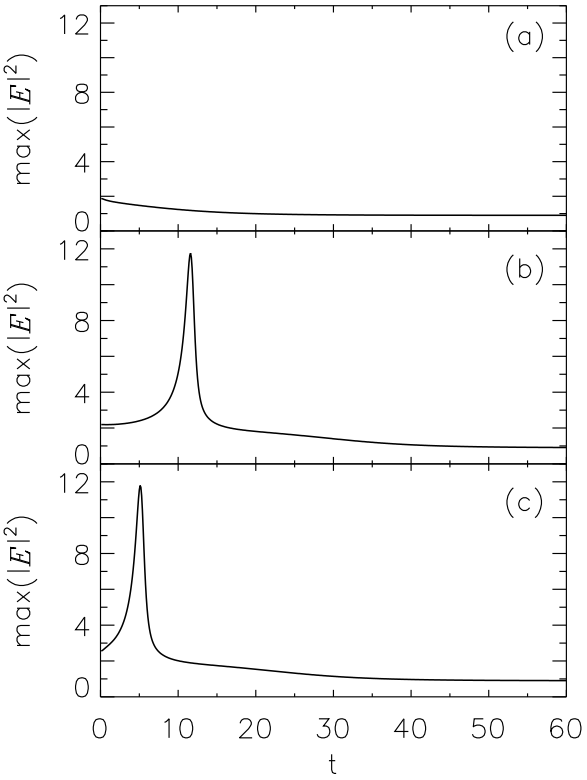

Fig. 3 Time evolution of the maximum intensity starting from the homogeneous solution plus a localized perturbation of the form of the unstable LS below (blue dashed line), just above (green solid line) and well above (red dotted line) threshold.

At this point it is worth noting that neglecting the spatial dependence Eq. (1) does not present any kind of excitability. The excitable behavior is an emergent property of the spatial dependence and it is strictly related to the dynamics of the 2D LS.

Finally, it is interesting to remark that the excitable region in parameter space is quite large and, potentially easy to observe experimentally. While this excitable behavior belongs to Class I (the period diverges to infinity when a perturbation hits the saddle), due to the logarithmic scaling law for the period (2), the parameter range

over which the period increases dramatically is extremely narrow. Therefore, from an operational point of view, systems exhibiting this scenario might not be classified as Class I excitable, as the large period responses may be easily missed [26].

4 Interaction of two oscillating localized states

In the previous section we have reviewed the dynamics of a single LS. In this one we study the interaction between two oscillating LS, and how it affects their dynamics. Oscillating LS are an example of *non-punctual oscillators*, i.e. oscillators with an internal structure. The interaction between such oscillatory structures through the tails can not be, in general, reduced to a simple coupling term between oscillators, but it modifies the internal structure of the oscillators themselves, affecting the dynamics in a nontrivial way. The interplay between the coupling and the internal structure of non-punctual oscillators is a general phenomenon not well understood. This chapter aims to be an approach to the subject.

We will first describe in section 4.1 the dynamics of two coupled oscillating LS in the full system, and then in section 4.2 we will study how much of the observed dynamics can be explained by means of a simple model for two coupled oscillators, and which effects can or can not be attributed to the spatial extension of the oscillators.

4.1 Full system

Throughout this section we will set $I_s \sim 0.84$, and $\theta = 1.27$ corresponding to a region of oscillatory structures [22, 19]. This value of I_s is close to the modulational instability that occurs at $I_s = 1$, and because of this LS have large tails. As the interaction between the structures is mediated by these tails, working in this region has the advantage that the interaction is strong and its effects are more evident.

Localized structures in this system have an intrinsic intensity profile with spatially oscillatory tails, and since the system is translationally invariant, the structures are free to move once created. When two stationary structures are placed close to each other, the presence of an adjacent structure sets only a discrete set of relative positions at which the structures can anchor, given by the intensity profile of the tails. Then if the structures are placed at arbitrary positions they will move until they sit at the zeros of the gradient of this intensity profile. This locking has been studied, both theoretically and experimentally, for stationary localized structures only [6, 7, 8].

Similarly to what happens with stationary LS, when two oscillatory localized structures are placed close to each other they move until they get locked by the tail interaction. For the selected parameters we observe three equilibrium distances that are $d_1 \sim 7.8, d_2 \sim 15.8$ and $d_3 \sim 19.9$. Beyond d_3 the interaction is so weak that the

structures can be considered as independent. The movement of the structures from an arbitrary position towards the equilibrium distances is very slow compared with the oscillation period. Therefore we will restrict ourselves to study the behavior of the system when the structures are at the equilibrium distances, to avoid long transient times and complex effects introduced by the movement of the LS.

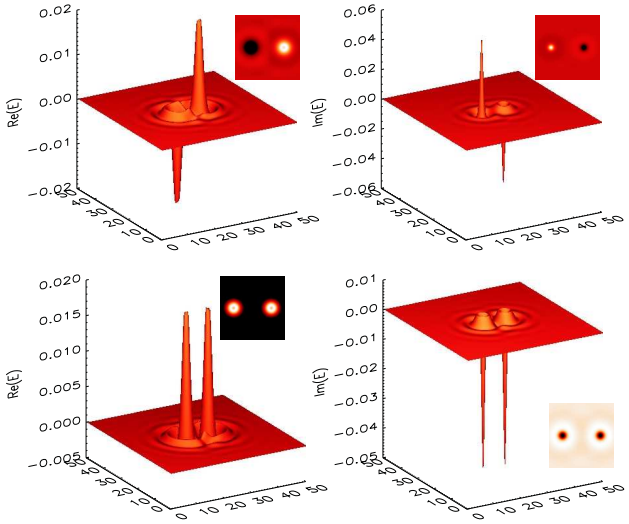

Fig. 4 Anti-phase (top) and in-phase (bottom) modes for $I_s = 0.86$ and $d = d_1 = 7.8$. These modes have been obtained from a full 2D linear stability analysis.

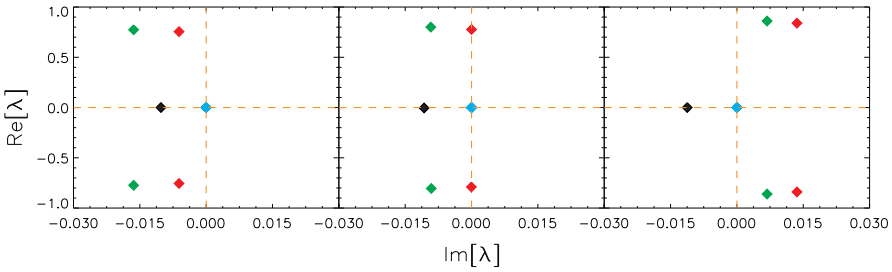

Fig. 5 Hopf bifurcation for two coupled LS at $d = d_1$. From left to right, Is=0.81,0.8266,0.83. Red and green dots are the eigenvalues corresponding to the anti-phase and in-phase modes respectively. The blue dots are three zero eigenvalues of the three Goldstone modes of the system of two LS, corresponding to global translations in the x and y directions, and to the rotation of the pair. The black dot is a damped mode associated with perturbations that modify the distance between the two LS.

A single LS undergoes a Hopf bifurcation at $I_s = 0.8413$ and starts to oscillate. At the bifurcation point this solution has then two complex conjugate eigenvalues whose real part becomes positive with an imaginary part different from zero. If we now consider two very far apart (non interacting) structures the system has globally two degenerate pairs of Hopf unstable eigenvalues. Since in this case the structures are independent from each other, they become simultaneously unstable at $I_s = 0.8413$ and the LS can oscillate at any relative phase.

If the two LS are now placed closer together, at one of the equilibrium positions, the structures are no longer independent. Now the interaction breaks the degeneracy of the spectrum splitting the eigenvalues in two different pairs of complex conjugates: a pair corresponding to in-phase oscillations and other to anti-phase oscillations (Fig. 4). Since the eigenvalues of these modes are no longer degenerate, increasing the driving, one of these two pairs will cross the Hopf bifurcation first (see Fig. 5). Because of the splitting, the threshold of the mode that become first unstable is, generically, lower that the threshold of the single LS. Physically this is due to the fact that the coupling can transfers energy from one LS to the other, such that the collective oscillation can have a lower threshold that a single LS. Although the splitting takes place mainly in the direction of the real axis, the imaginary part is also slightly modified, so the two new cycles have different frequencies. This degeneracy breaking mechanism is crucial to understand the interaction of these LS.

For $d = d_3$ the interaction is very weak, and the degeneracy is merely broken. The real part of the eigenvalues corresponding to the in-phase and anti-phase oscillations become positive almost simultaneously, although the in-phase cycle appears first at $I_s = 0.8412$, very close to the threshold of an isolated LS. As a result, the in-phase solution is stable close to the bifurcation and the anti-phase solution is created just after and it is unstable. The stability is, however, interchanged for larger values of the input intensity in favor of the antiphase solution. This is illustrated in Fig. 6a, where the bifurcation diagram of the in-phase and anti-phase cycles is shown for the third equilibrium distance d_3.

For $d = d_2$ the difference between the two pairs of eigenvalues is still very small but, this time, the anti-phase mode crosses the Hopf bifurcation first. The changes in the threshold are still almost imperceptible. The anti-phase solution remains then stable for all values of the input intensity (Fig. 6 b). In this case the inphase solution is always unstable.

Finally for $d = d_1$ the degeneration is completely broken, and the anti-phase mode crosses the Hopf bifurcation much before than the in-phase one, as shown in Fig. 5. For this the closest distance the interaction is quite strong and the situation is more complicated. First the stable anti-phase limit cycle is created at $I_s \simeq 0.8266$, much before that the threshold of an isolated LS. Initially, both structures have the same oscillation amplitude. At $I_s \simeq 0.828$ there is a symmetry breaking bifurcation and the oscillation amplitude of the two structures becomes different, i.e. the two structures oscillate around the same mean value in anti-phase but with different amplitudes (regime II in Fig. 6c). The difference in the oscillation amplitude between the two structures grows gradually with I_s. An interesting effect due to the extended nature of the solutions is that in this region the pair of LS moves due to the asym-

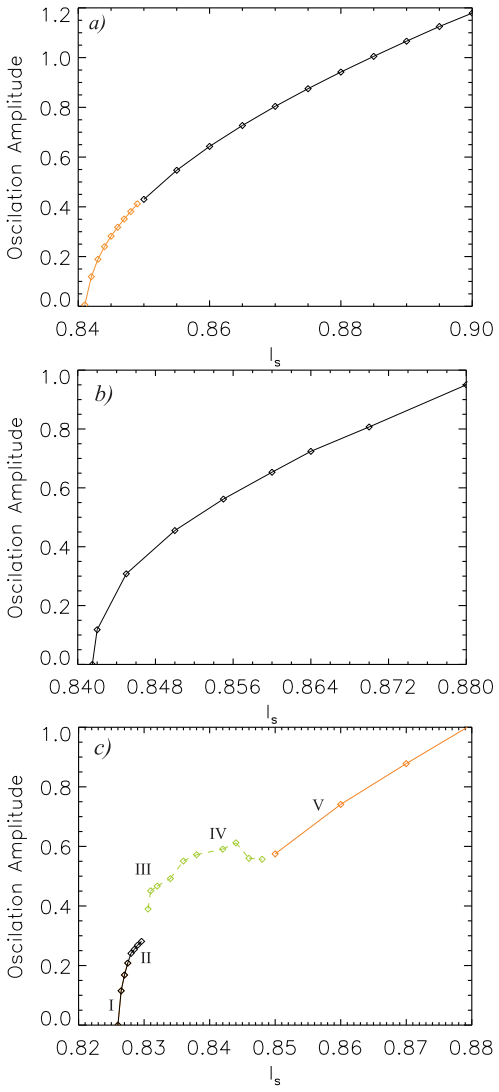

Fig. 6 Amplitude of the in-phase (orange), anti-phase (black) and mixed (green) oscillations as a function of I_s for the first three equilibrium distances: a) $d_3 = 19.9$, b) $d_2 = 15.8$, and c) $d_1 = 7.8$.

metry [27]. The centers of the two structures drift along the x axis in the direction of the structure with larger oscillation amplitude. For larger I_s the unstable in-phase limit cycle is created and it becomes stable at $I_s = 0.84$. In this case we observe also a third branch connecting the in-phase and anti-phase cycles corresponding to a mixed mode. Since the two cycles have a slightly different frequency, this mode presents a beating at the frequency difference of the in-phase and anti-phase modes.

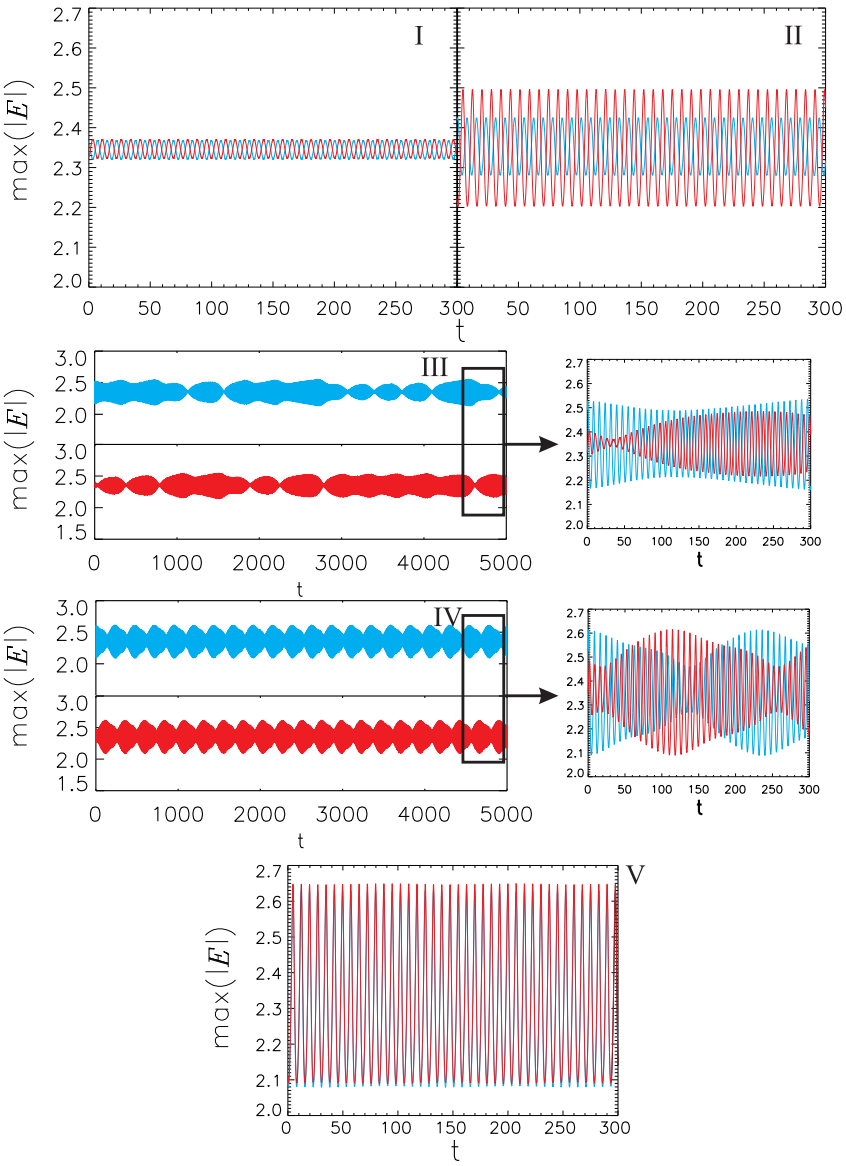

Fig. 7 Time traces of the maximum of the two LS for different values of I_s. Each panel corresponds to one of the tags of Fig. 6.

This situation is illustrated in detail in Fig. 7. Each of the panels in the figure corresponds to one of the tags in Fig. 6c, showing a time trace of each dynamical regime. Fig. 7 I shows the anti-phase oscillations. Increasing I_s, we reach the regime where the anti-phase oscillations are asymmetric (Fig. 7 II). Further increasing I_s the anti-phase cycle become unstable and the amplitude of the oscillations is modulated by a slow frequency. Close to the anti-phase cycle the fast oscillations of this modulated cycle are almost in anti-phase (Fig. 7 III). Near the end of this branch the fast oscillations are almost in phase (Fig. 7 IV). Finally, the amplitude of the modulations decreases until we reach a the regime of in-phase oscillations (Fig. 7 V).

4.2 Simple model: two coupled Landau-Stuart oscillators

As the oscillating LS are extended oscillators it is interesting to wonder which part of the dynamics observed in the previous subsection can be attributed to the extended nature of the LS and which one simply to two coupled oscillators. To try to discern these to components in the dynamics we consider a simple model describing two interacting limit cycle oscillators close to a Hopf bifurcation, namely two coupled Landau-Stuart (L-S) equations. We give some hints on how to determine the effective parameters of these pair of equations from the full system, and describe the different dynamical regimes that arise from them.

We try to understand, then, the interaction of two oscillating LS in terms of a phase-amplitude reduction of two subsystems close to a Hopf bifurcation. In their classical paper Aronson *et al.* [28] analyze this situation. They arrive to a center manifold reduction for two limit cycles that allows to write the interaction in terms for the complex amplitudes A_1 and A_2 of two Landau-Stuart oscillators,

$$\begin{aligned} \dot{A_1} &= A_1[\mu + i\omega - (\gamma + i\alpha)|A_1|^2] + (\beta + i\delta)(A_2 - \kappa A_1) \\ \dot{A_2} &= A_2[\mu + i\omega - (\gamma + i\alpha)|A_2|^2] + (\beta + i\delta)(A_1 - \kappa A_2) \end{aligned} \tag{3}$$

Here, for clarity, we have not rescaled the parameters of the oscillators and the only assumption we have done is that both oscillators are identical. With the presence of the parameter δ we consider the most general case of a nonscalar coupling (other authors also call it reactive, elastic or nondiagonal coupling). Physically, in a mechanical system, this couples momentum coordinates to position and/or viceversa. In optics this corresponds to the coupling associated to diffraction (in the paraxial approximation). Its most important consequence is that it couples amplitude with phase, breaking thus, the usual assumption that we can describe coupled oscillators only through their phases and neglecting amplitudes.

Another important ingredient that allows for a rich dynamical behavior is nonisochronicity, i.e., the nonlinear dependence of the frequency with the amplitude (also called shear or nonlinear frequency pulling in the literature) given by α. We note also that we have included, as in [28], the $\kappa \in [0,1]$ parameter, such that $\kappa = 1$

corresponds to the usual coupling (diffusive in the case that $\delta = 0$), while $\kappa = 0$ corresponds to direct coupling (no self-interaction term).

From these equations, using $A_{1,2} = R_{1,2}\exp(i\theta_{1,2})$, one can obtain the following equations in polar coordinates

$$\dot{R_1} = R_1(\mu - \beta\kappa - \gamma R_1^2) + R_2(\beta\cos\psi - \delta\sin\psi) \tag{4}$$

$$\dot{R_2} = R_2(\mu - \beta\kappa - \gamma R_2^2) + R_1(\beta\cos\psi + \delta\sin\psi) \tag{5}$$

$$\dot{\psi} = \alpha(R_1^2 - R_2^2) - \beta\sin\psi\left(\frac{R_1}{R_2} + \frac{R_2}{R_1}\right) + \delta\cos\psi\left(\frac{R_1}{R_2} - \frac{R_2}{R_1}\right) \tag{6}$$

where the phase difference $\psi = \theta_2 - \theta_1$ is the only relevant angular variable, due to the invariance symmetry under transformations with respect to the global phase exhibited by the evolution equations.

Let us first analyze the two symmetric solutions, with $R = R_1 = R_2$, the in-phase and the anti-phase solutions. As they are fixed point solutions, both of them satisfy

$$\mu - \beta\kappa - \gamma R^2 + \beta\cos\psi = 0 \tag{7}$$

or,

$$R^2 = [\mu + \beta(1-\kappa)]/\gamma \tag{8}$$

for the in-phase solution ($\psi = 0$), and

$$R^2 = [\mu - \beta(1+\kappa)]/\gamma \tag{9}$$

for the anti-phase one ($\psi = \pi$). As the amplitude (squared) for an uncoupled oscillator is $R_u^2 = \mu/\gamma$, we note that, for positive β (attractive coupling), except for the so-called diffusive coupling ($\kappa = 1$), the amplitude of the in-phase solution is *bigger* than the amplitude of an uncoupled oscillator. The opposite would happen for repulsive coupling $\beta < 0$. Similarly, for attractive coupling ($\beta > 0$) the amplitude of the anti-phase synchronized solution is *smaller* compared with the uncoupled oscillator (the opposite would happen for repulsive coupling).

4.2.1 Estimation of parameters I

From the previous results one gets a procedure to determine some effective parameters from the full model. Comparing the amplitudes of the in-phase and anti-phase symmetric solutions, and keeping all parameters fixed, from Eqs. (8) and (9) one gets

$$\begin{aligned} R_{inp}^2 - R_u^2 &= \beta(1-\kappa)/\gamma \\ R_u^2 - R_{antip}^2 &= \beta(1+\kappa)/\gamma \end{aligned} \tag{10}$$

where R_u is the amplitude of single uncoupled oscillator, and R_{inp} and R_{antip} are the amplitudes of the in-phase and anti-phase limit cycles respectively. As shown in

Fig. 6, R_{inp} and R_{antip}, as well as R_u, can easily be calculated from the numerical integration of the full model (1). Then, κ and β/γ can be obtained from the system of two equations (10):

$$Q = \frac{R_{inp}^2 - R_u^2}{R_u^2 - R_{antip}^2} = \frac{1-\kappa}{1+\kappa}$$

$$\kappa = \frac{1-Q}{1+Q} \tag{11}$$

$$\frac{\beta\kappa}{\gamma} = R_u^2 - \frac{1}{2}(R_{inp}^2 + R_{antip}^2) \tag{12}$$

We note that measuring R_u, R_{inp} and R_{antip} for the same values of the parameters require working in a region of coexistence between in-phase and anti-phase oscillations. This is not necessarily possible and the stability of the two limit cycles must be first checked. Nevertheless in some cases it is possible to measure R_{inp} or R_{antip} even if one of these solutions is unstable. In order to do so, the growth rate of the unstable mode must be much slower that the frequency of the cycle, so that starting from an initial condition close to the unstable solution one can observe several oscillations where the radius does not change significantly.

We have also assumed here that κ, as well as β and δ are the same for the in-phase and anti-phase solutions. This is again not guaranteed, due to the spatial nature of the oscillators, and the coupling could depend explicitly on the shape of the solutions. In any case, for weak interaction (long distance between oscillators) this should be a reasonable first order approximation.

4.2.2 Estimation of parameters II: quenching experiments

In [29] Hynne and Sorensen reported a method to determine the coefficients of the cubic term of the Landau-Stuart normal form of a Hopf, namely γ and α. This is based on a so-called quenching experiment[1], in which one makes a perturbation of a system sitting on a stable limit cycle to make it jump momentarily on the unstable fixed point (focus) in its center. One then measures quantitatively the return of the trajectory to the limit cycle attractor. The procedure goes as follows. One starts with a single, uncoupled, Landau-Stuart oscillator,

$$\dot{A} = A[\mu + i\omega - (\gamma + i\alpha)|A|^2], \tag{13}$$

or in polar representation

$$\dot{R} = R(\mu - \gamma R^2) \tag{14}$$

$$\dot{\theta} = \omega - \alpha R^2, \tag{15}$$

[1] A theory of quenching is presented in [30]

being the limit cycle defined by $R_u = \sqrt{\mu/\gamma}$ and the unstable focus at its center by $R = 0$. Then, one can determine the slope $s_{1/2}$ of the tangent to a time series of the radius at the half amplitude point $R = R_u/2$ (see Fig. 8) from a quenching experiment. Using Eq. (14),

$$s_{1/2} = \left.\frac{dR}{dt}\right|_{R=R_u/2} = \frac{\mu R_u}{2} - \frac{\gamma R_u^3}{8} = \frac{\gamma R_u^3}{2} - \frac{\gamma R_u^3}{8} = \frac{3}{8}\gamma R_u^3$$

and γ can be determined as,

$$\gamma = 8 s_{1/2}/3R_u^3. \tag{16}$$

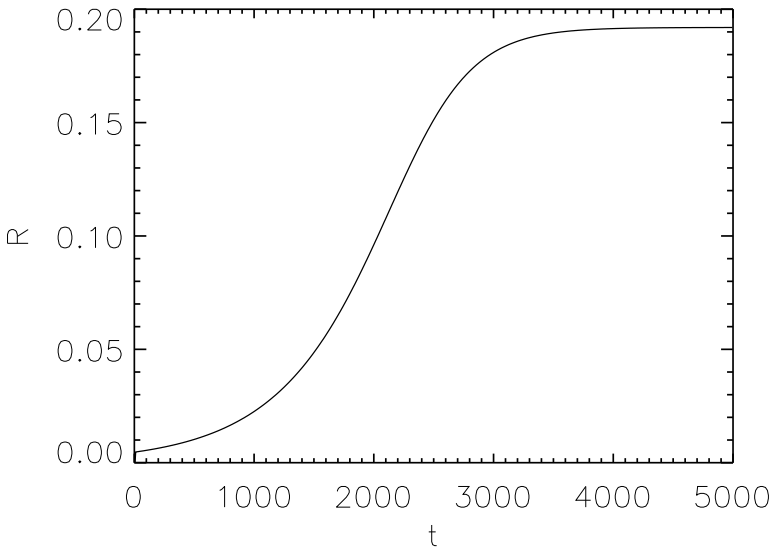

Fig. 8 Time trace of the maximum of a LS (R) in a quenching experiment starting from the unstable focus.

To determine the nonisochronicity α one has to analyze the dynamics of the phase θ. From Eq. (15) one obtain that

$$\alpha = \Delta\omega/R_u^2 \tag{17}$$

where $\Delta\omega$ is the difference between the frequency of *infinitesimally small oscillations* and the frequency of the stable limit cycle. The frequency of the small oscillations around the unstable fixed point is given by the imaginary part of the unstable eigenvalue of the focus, which can be determined exactly from a linear stability anal-

ysis. The frequency of the stable limit cycle is easily determined from a numerical simulation of the full system.

Finally, knowing how to determine γ, β can be obtained from (12), and μ can also be easily estimated from the amplitude of the limit cycle R_u. Thus, all the parameters of the system have been estimated, except for the reactive coupling coefficient δ, determined in the next section.

4.2.3 Estimation of δ

To obtain the reactive coupling coefficient δ one needs to study the relaxation of two coupled oscillators to a stable limit cycle after an asymmetric perturbation. In particular, it can be seen that the dynamics of the two oscillators close to the limit cycle depends directly on the value of δ [31]. Then, to determine this coefficient we have performed systematically simulations of the simple model starting from the same asymmetric initial condition, and different values of δ. We then compare the results with a simulation of the full model where the two LS have been initialized with equivalent phases and radius than the two Landau-Stuart equations, and we choose the value of δ that better fits the dynamics of the full system.

Fig. 9 shows the evolution of the full and simple models for equivalent initial conditions and the best value of δ. There is a very good agreement between the dynamics of the two models, although this is the most difficult and less accurate estimation of all.

4.2.4 Results and dynamical regimes of the simple model

As a result of the procedures described above, we obtained the following parameters for the largest distance d_3:

I_s	μ	κ	γ	α	β
0.843	0.0015843930	2.26433	0.04300	-0.26699925	2.97237×10^{-5}
0.845	0.0034164778	1.89287	0.04256	-0.28231057	3.51847×10^{-5}
0.847	0.0052667790	1.63081	0.04249	-0.27617558	3.93145×10^{-5}
0.849	0.0070653138	1.51109	0.04208	-0.27851949	4.09333×10^{-5}
$\delta = 9\times10^{-5}$					

Table 1 Estimated parameters for $d = d_3$.

For these parameters the dynamics of the two Landau-Stuart equations acceptably reproduce the dynamics observed for d_3 and, possibly for d_2. Fig. 10 shows the results of the stability analysis of the in-phase and anti-phase solutions of Eq. (3) for the parameter values given in Table 1. For small positive values of δ the in-phase solution is stable, while the anti-phase solution is unstable. The opposite situation occurs for small negative values of δ. In the previous Section we estimated

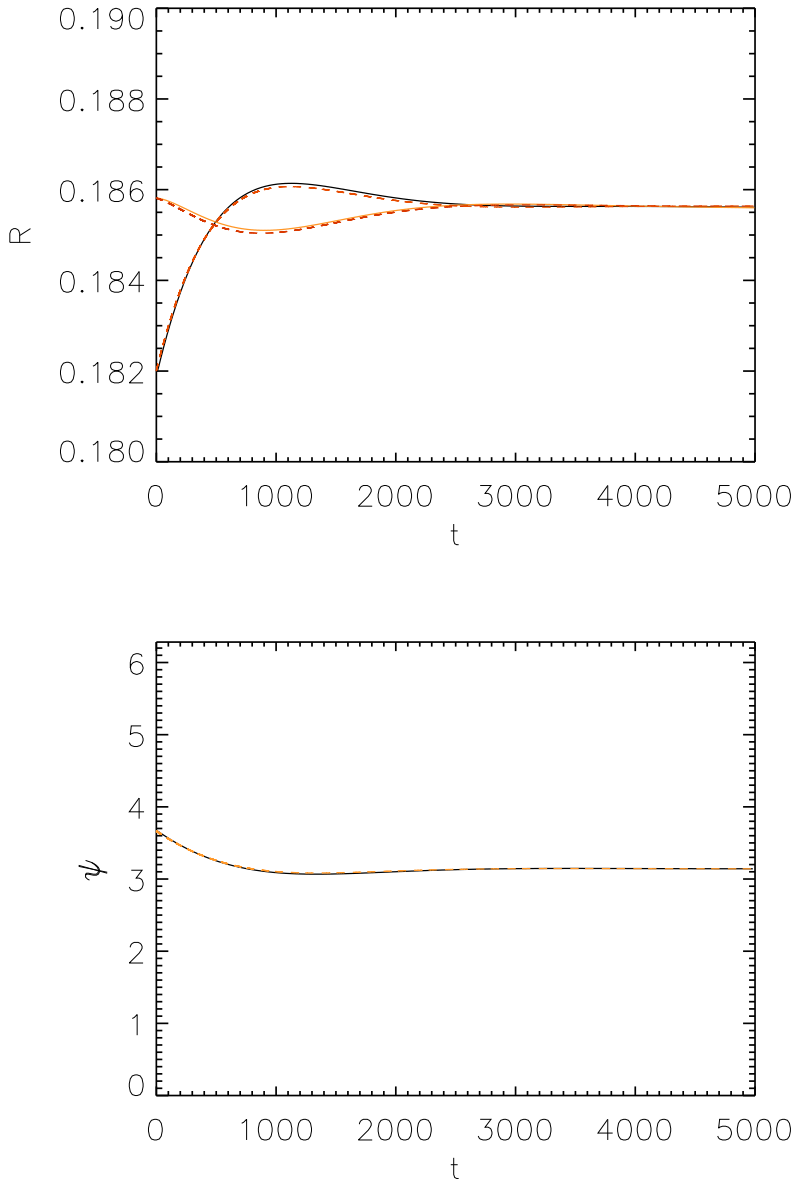

Fig. 9 Time evolution of the radius R of each oscillator, and their relative phase ψ, for the full system (solid lines) and the simple model of two coupled Landau-Stuart equations (dashed lines) after applying an asymmetric perturbation to the stable anti-phase limit cycle. For the right value of δ there is a very good agreement between the evolution of the two systems.

$\delta = 9 \times 10^{-5}$, which is in agreement with the fact that for $d = d_3$ we observe the in-phase solution to be stable close to the Hopf bifurcation while the anti-phase solution is unstable, although the simple model do not capture the interchange of stability observed in the full model for larger values of the input intensity. The estimation of δ is, however, not very accurate and since the value of δ is so small, the error bars would include both positive and negative values. Nevertheless, the fact that we find δ to be close to zero makes possible the fact that for $d = d_2$ we observe the opposite situation than for $d = d_3$, namely that the anti-phase solution is stable and the in-phase solution unstable, although we have not estimated the parameters for that distance.

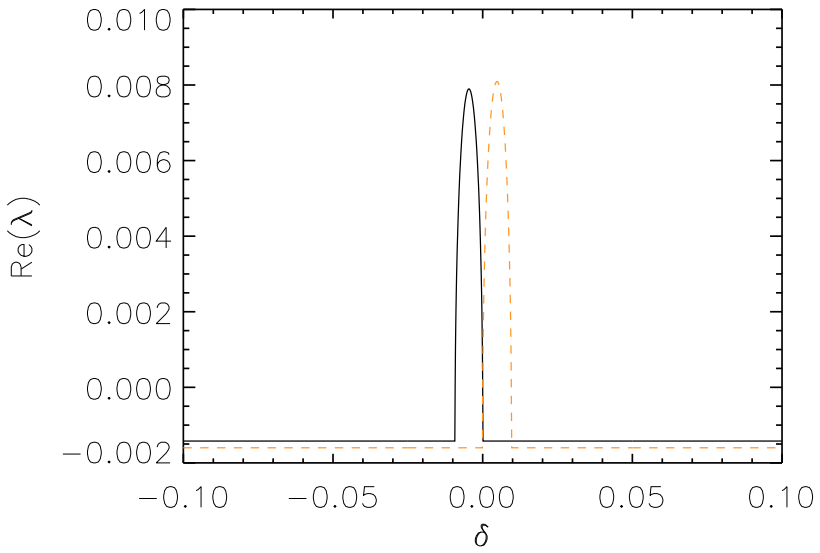

Fig. 10 Real part of the eigenvalues of the in-phase (solid line) and anti-phase (dashed line) limit cycles of the two coupled Landau-Stuart equations as a function of δ for the estimated parameters (Table 1).

In principle, this approach assumes that the only parameters that change from one distance to another are those associated with the coupling, i.e. α, β and κ, while those of an isolated oscillator remain the same. In the case of $d = d_1$, the interaction is so strong that we can not use the techniques explained above to estimated the parameters. We have then explored numerically different values of the parameters of the coupling, but we have not found any region where the simple model can exactly reproduce the dynamics of the full model for $d = d_1$. This seems to indicate that this approach is to simple for this case and that the spatial extension of the oscillators do play a role in the complex dynamics. Possibly, the interaction changes

somehow the effective values of the parameters of the individual oscillators, or even more, these parameters may not even be constant at all. It is still possible, however, that for more remote effective parameter values, the system of two coupled Landau-Stuart Equation can reproduce, at least partially, the observed regimes, but this needs further investigation.

5 Interaction of excitable localized states: logical gates

In this section we explore the possibility of using excitable localized structures to perform logical operations. Computational properties of waves in chemical excitable media (e.g. the Belousov-Zhabotinsky reaction) have been used to solve mazes [32], to perform image computation [33], and also logic gates have been constructed from these (chemical) systems [34, 35, 36]. After all, excitability is a property exhibited by neurons and used by them to perform useful computations [37] in a different way than the more usual attractor neural networks [38, 39].

Optical computing, via photons instead of electrons, has long appealed researchers as a way of achieving ultrafast performance. Photons travel faster than electrons and do not radiate energy, even at fast frequencies. Despite the constant advances and miniaturization of electronic computers, optical computing remains a strongly studied subject. Probably the strategy to follow is not to seek to imitate electronic computers, but rather to try to fully utilize the Physics of these systems, e.g., their intrinsic parallelism.

Most of the systems studied in optical computing applications imply light propagation, for example optical correlators, already commercially used in optical processing applications [40]. Instead, with the goal of designing more compact optical schemes, localized structures have emerged as a potentially useful strategy for information storage, where a bit of information is represented by a LS. One can take this idea a step further and discuss the potential of LS, for carrying out computations, i.e., not just for information storage. In particular, logic gates can be designed using LS. We will show here how an AND and OR gates can be implemented using three excitable LS.

To make use of the excitable regime we use a set of addressing Gaussian beams that allow us to set precisely the distance between excitable spots and control the excitable threshold of each one [41]. Strictly speaking this Gaussian beam changes slightly the scenario, but the underlying physics remains basically the same as described in section 3.3. So, to design a logical gate, we set three addressing beams at proper distances and intensities such that their interaction creates a dynamics whose response to two input perturbations is given by Table 2 reproducing an AND and an OR logical gates.

In particular we consider three excitable LS in a linear arrangement, with a separation d between them. Three permanent Gaussian localized beams are applied: I_{sh}^{I1} and I_{sh}^{I2} at each side for the input LS, and I_{sh}^{O} in the middle for the output LS. The Gaussian beams fix the spatial position of input and output LS. If there is an ex-

	Input 1	Input 2	Output
OR	0	0	0
	1	0	1
	0	1	1
	1	1	1
AND	0	0	0
	1	0	0
	0	1	0
	1	1	1

Table 2 Truth Table of AND and OR logic gates.

citable excursion in the central localized structure the output is interpreted as a "1" and if there is no excitable response as a "0". At the input, superthreshold perturbations (i.e. causing an excitable excursion) correspond to a bit "1", while subthreshold (or the absence of) perturbations will be considered as a bit "0". Physically, the interaction is mediated by the tails of the structures and the remnant wave that radiate from the LS dissipating the energy to the surroundings during the excitable excursion.

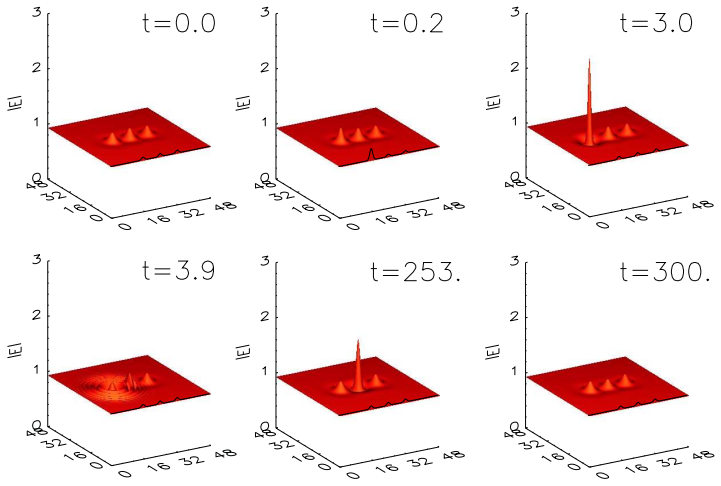

Fig. 11 Resonse of an OR logic gate to a ("1", "0") input.

Then, if the distance d between the input LS and the output is small enough, such that the excitable excursion of a single LS at the input is enough to excite an excursion at the output we will have an OR gate. To avoid that the output can excite the input LS I_{sh}^{I1} and I_{sh}^{I2} are smaller than I_{sh}^{O}, so that the excitable threshold of the input LS is too high to be excited by the excitable excursion of the output LS. If we simply make d larger so that the interaction of a single LS is not enough to excite

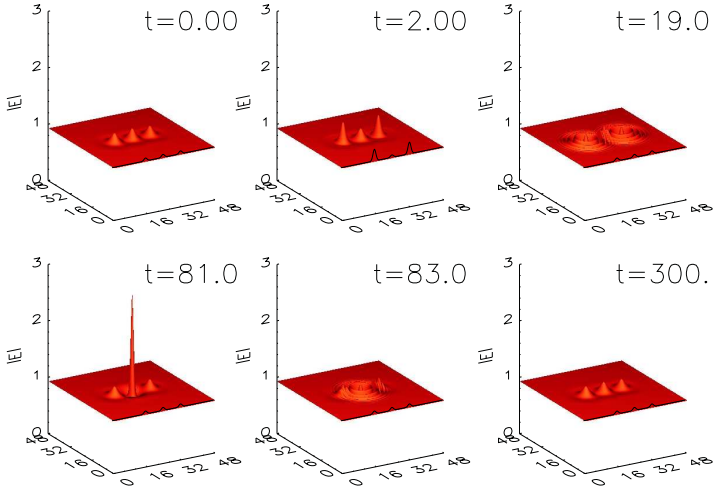

Fig. 12 The same as in Fig. 11 for a (“1”, “1”) input.

the output, but the combined effect of the two input LS is, we have implemented an AND gate according to Table 2.

Fig. 11 shows the dynamics or an OR gate for a (“1”, “0”) input. Applying a similar perturbation to I_{sh}^{I2} [corresponding to (“0”, “1”)], the same result is obtained. Finally, if we simultaneously apply the same perturbation to both I_{sh}^{I1} and I_{sh}^{I2} [corresponding to (“1”, “1”)], a similar excitable excursion is obtained for the central (output) LS, as shown in Fig. 12.

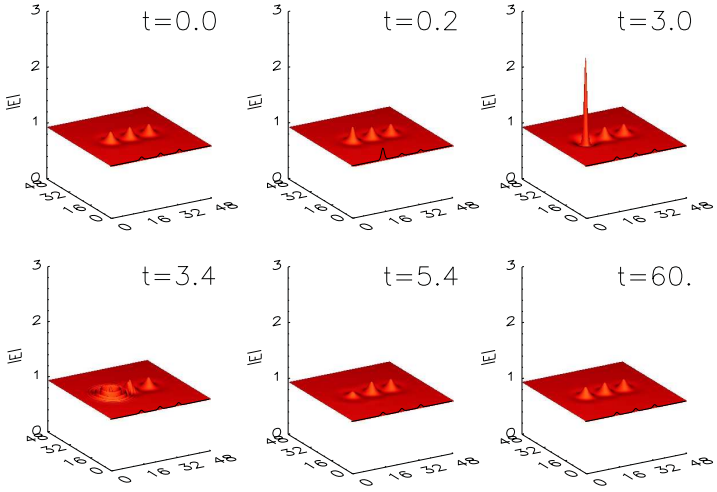

Fig. 13 Response of an AND logic gate to a (“1”, “0”)input.

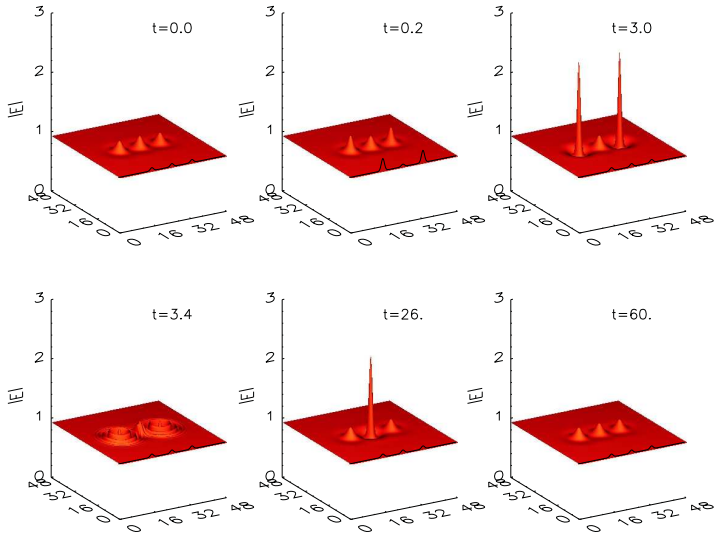

Fig. 14 The same as in Fig. 13 for a (“1”, “1”) input.

Figs. 13 and 14 show the response of an AND gate to a (“1”, “0”) and a (“1”, “1”) inputs respectively.

With these two basic gates combined with a NOT gate, not explained here, it is possible to build the two universal logic gates, NAND and NOR, which are the pillars of logic. In electronics, these gates are built from transistors, but they can be built by means of other technologies. We propose here using excitable LS. We have to note, however, that using excitability to perform computations may imply relatively long times inherent to the slow dynamics close to a fixed point. This drawback can be minimized by properly tuning the parameters of the system and optimizing the form of the perturbations. The aim of this work is just setting the basis of a new way to perform all-optical logical operations using localized states.

6 Summary

It is remarkable how such a simple model as (1) can show such a rich and surprising behavior through the dynamics of coherent structures. In particular, localized states show different emergent behavior that can not be explained in terms of the local dynamics of the model, but it is a self-organized phenomenon due to the spatial coupling provided by diffraction. In the first part, we have briefly reviewed two instabilities, namely a Hopf and a saddle-loop bifurcation, that signal the boundaries between three different dynamical regimes: stationary, oscillatory and excitable. An extensive analysis of this scenario can be found in [1].

Then, we have focused in the study of the interaction between two LS in the oscillatory regime. We have shown how the interaction breaks the degeneracy of the spectrum of two LS creating two limit cycles with slightly different frequencies. These two cycles bifurcate also for slightly different values of the control parameter and they correspond to in-phase and anti-phase oscillations. An important issue addressed in this section is the role of the internal structure of LS in the dynamics. For long distances between LS, i.e. weak interaction, we have shown that the dynamics can be reasonable explained by means of two simple coupled oscillators. We have given a simple model and described a method to estimated its parameters from the dynamics of the full system. For the closest distance, however, we observe a much more complex dynamics, and the simple model does not reproduce this behaviour, at least for the adjusted parameters. This seems to indicate that the internal degrees of freedom play a role in the dynamics and that interaction couples, for instance, the movement in the transverse plain with the oscillations.

Finally, in the last section, we have shown how coupling several LS in the excitable regime, one can perform logical operations. This opens the possibility to build new all-optical components to process information based on the use of LS.

References

1. P. Colet, D. Gomila, A. Jacobo, M.A. Matías, *Dissipative Solitons: From Optics to Biology and Medicine* (N. Akhmediev and A. Ankiewicz, eds.) , Springer-Verlag, 113-136 (2008).
2. F.T. Arecchi, S. Boccaletti, and P. Ramazza, Phys. Rep. **318** 1 (1999).
3. L.A. Lugiato, M. Brambilla, and A. Gatti, Adv. Atom. Mol. Opt. Phys. **40** 229 (1999).
4. W.J. Firth and C.O. Weiss, Opt. Photon. News **13** 55 (2002).
5. T. Ackemann, W.J. Firth, and G.-L. Oppo, Adv. Atom. Mol. Opt. Phys. **57** 323 (2009).
6. B. Schäpers, T. Ackemann and W. Lange, Phys. Rev. Lett. **85**, 748 (2000); J. Opt. Soc. Am. B **19**, 707 (2002).
7. P. L. Ramazza, E. Benkler, U. Bortolozzo, S. Boccaletti, S. Ducci, and F. T. Arecchi, Phys. Rev. E **65**, 066204 (2002).
8. P. L. Ramazza, U. Bortolozzo, and S. Boccaletti, Appl. Phys. B **81**, 921 (2005).
9. D. Michaelis, U. Peschel, and F. Lederer, Opt. Lett. **23** 1814 (1998).
10. W. J. Firth, G. K. Harkness, A. Lord, J. M. McSloy, D. Gomila, and P. Colet, J. Opt. Soc. Am. B **19**, 747 (2002).
11. L.A. Lugiato and R. Lefever, Phys. Rev. Lett. **58** 2209 (1987).
12. W.J. Firth, A. Lord, and A.J. Scroggie, Physica Scripta **67**, 12 (1996); W.J. Firth and A. Lord, J. Mod. Optic. **43**, 1071 (1996).
13. A. J. Scroggie, W. J. Firth, G. S. McDonald, M. Tlidi, R. Lefever, and L. A. Lugiato, Chaos, Solitons Fractals **4**, 1323 (1996).
14. D. Gomila and P. Colet, Phys. Rev. A **68**, 011801R (2003).
15. D. Gomila and P. Colet, Phys. Rev. E **76**, 016217 (2007).
16. P. D. Woods and A. R. Champneys, Physica D **129**, 147 (1999).
17. P. Coullet and C. Riera and C. Tresser, Phys. Rev. Lett. **84**, 3069 (2000).
18. J. M. McSloy, W. J. Firth, G. K. Harkness, and G. L. Oppo, Phys. Rev. E **66**, 046606 (2002).
19. D. Gomila, A. Jacobo, M. A. Matías and P. Colet, Phys. Rev. E **75** 026217 (2007).
20. D. V. Skryabin, J. Opt. Soc. Am. B **19**, 529 (2002).
21. D. Gomila, A.J. Scroggie, and W.J. Firth, Physica D **227**, 70 (2007).
22. D. Gomila, M. A. Matías and P. Colet, Phys. Rev. Lett. **94**, 063905 (2005).

23. P. Glendinning, Stability, Instability, and Chaos (Cambridge University Press, Cambridge, England, 1994).
24. P. Gaspard, J. Phys. Chem. **94**, 1 (1990).
25. E. M. Izhikevich, Int. J. Bifurcation Chaos Appl. Sci. Eng. **10**, 1171 (2000).
26. E. M. Izhikevich, Dynamical Systems in Neuroscience (MIT Press, Cambridge, MA, 2006).
27. A.J. Scroggie, D. Gomila, W.J. Firth, and G.-L. Oppo, Appl. Phys. B **81**, 963 (2005).
28. D.G. Aronson, G.B. Ermentrout, and N. Kopell, *Amplitude response of coupled oscillators*, Physica D **41**, 403-449 (1990).
29. F. Hynne and P.G. Sorensen, *Experimental determination of Ginzburg-Landau parameters for reaction-diffusion systems*, Phys. Rev. E **48**, 4106 (1993).
30. F. Hynne, P.G. Sorensen, and K. Nielsen, *Quenching of chemical oscillations: General theory*, J. Chem. Phys. **92**, 1747 (1990).
31. A. Pikovsky, M. Rosenblum, and J. Kurths, *Synchronization*, (Cambridge U.P.,2001).
32. O. Steinbock, A. Tóth, and K. Showalter, Science **267**, 868 (1995).
33. L. Kuhnert, K. I. Agladze, and V. I. Krinsky, Nature **337**,244 (1989).
34. A. Toth and K. Showalter, J. Chem. Phys. **103**, pp. 2058, (1995).
35. O. Steinbock, P. Kettunen, and K. Showalter, J. Phys. Chem. **100**, 18970 (1996).
36. J. Gorecka and J. Gorecki, J. Chem. Phys. **124**, 084101 (2006).
37. C. Koch, *Biophysics of Computation* (Oxford U.P., Oxford, 1999).
38. W. S. McCulloch and W. H. Pitts, Bull. Math. Biophys. **5**, 115 (1943).
39. D. J. Amit, *Modeling brain function* (Cambridge U.P., Cambridge, 1989).
40. E. J. Lerner, Laser Focus World **1**, 99 (2000).
41. A. Jacobo, D. Gomila, M.A. Matías, and P. Colet, Phys. Rev. A **78**, 053821 (2008).